ELSEVIER

International Journal of Mass Spectrometry 197 (2000) 149–161

International Journal of Mass Spectrometry

Secondary ion emission from keV energy atomic and polyatomic projectile impacts on sodium iodate

M.J. Van Stipdonk[a,*], V. Santiago[a], E.A. Schweikert[a], C.C. Chusuei[b], D.W. Goodman[b]

[a]*Center for Chemical Characterization and Analysis, Department of Chemistry, Texas A&M University, College Station, TX 77843-3144, USA*

[b]*Department of Chemistry, Texas A&M University, P.O. Box 30012, College Station, TX 77843-3012, USA*

Received 18 August 1999; accepted 11 October 1999; revised 6 October 1999

Abstract

Sodium iodate and sodium iodide are inorganic solids in which iodine exists in different chemical environments. In sodium iodate, the iodine atom is bonded to oxygen to make the trigonal pyramidal IO_3 anion, which in turn is incorporated with sodium into an ionic crystal. In sodium iodide, however, the iodide anion and sodium cation are ionically bound in a crystal lattice. Nearly half of the negative secondary ion yield generated from keV energy polyatomic ion impacts on a sodium iodate surface is characteristic of ion emission expected from sodium iodide (i.e. $(NaI)_nI^-$), yet x-ray photoelectron spectroscopy data indicate that the solid material resulting from aliquots of aqueous sodium iodate dried on stainless steel contains no more than 2% sodium iodide. To determine how the number of atoms in the primary ion influences the amount of iodide type ion formation from sodium iodate, secondary ion yield measurements were performed using Cs, (CsI)Cs, and $(CsI)_2Cs$ projectiles incident at energies ranging from 10 to 25 keV. The experiments were run on an event-by-event basis at the level of single ion impacts. The yields of iodate (composed of Na, I, and O) and iodide type secondary ions increase with the energy of the projectile and the number of constituent atoms. When compared on a per-incident atom basis, however, we found that the yields of secondary ions characteristic of iodate saturate at three total projectile atoms, but continue to increase nonlinearly for iodide species (i.e. the yield per impacting atom increases). (Int J Mass Spectrom 197 (2000) 149–161) © 2000 Elsevier Science B.V.

Keywords: Ion formation; Polyatomic primary ions; Chemical damage, Secondary ion mass spectrometry; Yield enhancements

1. Introduction

Secondary ion mass spectrometry (SIMS) is an effective tool for determining the elemental composition of organic, inorganic, and metallic surfaces [1]. The introduction of polyatomic primary ion beams has improved the performance of SIMS for the characterization of surface molecular species [2–8]. This is primarily due to the significantly higher yields (defined here as the number of secondary ions detected per primary ion impact) of polyatomic and molecular secondary ions produced by polyatomic primary ions over the atomic projectiles traditionally used in SIMS such as Ar, Xe, and Cs.

Evaluating the use of SIMS to determine the chemical composition and structure of solid surfaces, par-

* Corresponding author.

PII S1387-3806(99)00255-9

ticularly of complex inorganic materials, has been an ongoing focus of our research effort. While the enhanced ion yields provided by polyatomic primary ion impact may benefit surface analysis using SIMS, recent work has demonstrated that cluster projectiles will increase the yield of secondary ions characteristic of chemical damage relative to those that reflect surface composition [9,10]. In particular, the yields of damaged ions are sensitive to the number of constituent atoms in the primary ion. In some cases, the chemical damage caused by individual polyatomic ion impacts is reminiscent of damage effects observed at high primary beam dose, i.e. beyond the static SIMS limit of $\sim 10^{12}$ ions/cm^2 [10]. Our goal is to gain a fundamental understanding of the chemical and physical processes that underlie secondary ion formation following polyatomic primary ion impacts. This will allow us to identify and apply polyatomic primary ions that produce high analytically useful secondary ion yields and minimal ion formation characteristic of chemical damage.

In this study, SIMS using atomic and polyatomic primary ions, and x-ray photoelectron spectroscopy (XPS) were used to characterize sodium iodate ($NaIO_3$) and sodium iodide (NaI) targets. $NaIO_3$ was chosen as a model target in this study because the negative ion mass spectra contain peaks that fall into two general categories. The first category of ions, composed of Na, I, and O, resemble the stoichiometry of $NaIO_3$ and thus accurately characterize the chemical composition of the solid material. The second category contains ions composed of only Na and I, and matches the ion signal generated from ion impacts on sodium iodide. To gain a better understanding of the influence of primary projectile characteristics (complexity and energy) on the formation and yield of the secondary ions in both categories, the relative yields produced by the impacts of Cs^+, $(CsI)Cs^+$, and $(CsI)_2Cs^+$ ions were measured at incident energies ranging from 10 to 25 keV. XPS was used to monitor the composition of duplicate $NaIO_3$ and NaI surfaces to determine the contribution of $(NaI)_nI^-$ formation from sodium iodide domains that may form within sodium iodate during sample preparation.

2. Experimental

2.1. Sample preparation

Sample targets for the secondary ion yield measurements were prepared using 0.3 M aqueous $NaIO_3$ and NaI (Aldrich Chemical, St. Louis, MO) solutions. Ten μL of the respective solutions were applied to individual stainless steel sample supports (surface area approximately 3 cm^2) and allowed to dry in a dark fume hood at ambient temperature. At this concentration, homogeneous coverage of the stainless steel support was achieved with minimal caking or crust formation. Five targets were prepared from the same sample solution and analyzed individually by mass spectrometry. The ion yields measured were reproducible within a particular sample to within $\pm$5% relative standard deviation (RSD) and $\pm$ 10% from sample to sample.

As for the SIMS analysis, samples for characterization by XPS were prepared by applying 10 μL aliquots for 0.3 M NaI and $NaIO_3$ solutions to individual stainless steel substrates (1 cm^2 surface area). It was not possible to use the same sample substrate in both the SIMS and XPS instruments. To maintain the integrity of the SIMS and XPS comparison, the same stainless steel stock material was used to construct both the SIMS and XPS sample substrates. Care was taken to prepare $NaIO_3$ sample targets for the XPS measurement exactly as for the ion yield measurements: samples for both measurements were prepared at the same time using the same stock solutions.

2.2. Mass spectrometry

Mass spectra from keV atomic and polyatomic and MeV atomic ion impacts were acquired using a dual time of flight (ToF) mass spectrometer. The configuration and operation of the instrument has been discussed in detail elsewhere [2]. $(CsI)_nCs^+$ (n = 0–2) primary ions were produced by the impacts of ^{252}Cf fission fragments on a aluminized mylar foil coated with a vapor deposited layer of cesium iodide. The

complementary fission fragment was used to start the ToF timing electronics.

The experiments described in this article were carried out in the event-by-event bombardment and detection mode at the limit of single projectile impacts. Ions sputtered from the source foil (for instance, H^+, Cs^+, and $(CsI)_2Cs^+$ may all be sputtered by a single fission fragment impact) by fission fragments were accelerated and separated in a primary drift region; no primary ion selection was performed. The impact energy for the $(CsI)_nCs$ primary ions ranged from 10 to 25 keV. Fission fragments that pass through the source foil and traverse the primary ion flight region will also strike the sample, providing the opportunity to collect plasma desorption and keV ion induced mass spectra in a single experimental run. To ensure that less than one projectile of a given *m/z* ratio impacted the sample target per start pulse the primary ion transmission was decreased to ~10% using low transmission grids.

After traversing the drift region the primary ions successively struck the sample target. Secondary electrons emitted from the target surface following primary ion impact were steered by a weak magnetic field into a detector. It is assumed that the secondary electron yield from the target surface is proportional to the number of primary ion impacts. Accordingly, the secondary electrons were used as a relative measure of the number of each primary projectile incident on the target surface. The secondary ions emitted from the target surface were accelerated to −7 keV, separated, and detected in a secondary drift region.

A coincidence counting protocol was used to simultaneously record and arrange the secondary ions detected from each relevant primary ion into individual secondary ion mass spectra [11]. Because of the event-by-event nature of these experiments, coincidence counting provided the primary ion mass selection. Relative secondary ion yields (not corrected for transmission and detection efficiency) were calculated by dividing the integrated peak areas from a given primary ion impact by the integrated secondary electron peak area from the same incident primary ion (following appropriate background subtraction). The ion yields produced by different projectiles could be directly compared because the transmission and detection efficiencies and the target surface conditions remained constant throughout the course of the experiment.

2.3. X-ray photoelectron spectroscopy

XPS measurements were performed in an ion-pumped Perkin-Elmer PHI 560 system using a PHI 25-270AR double-pass cylindrical mirror analyzer. A Mg $K\alpha$ anode operated at 12 kV and 200 W with a photon energy of $h\nu = 1253.6$ eV was used as the excitation source. The vacuum system base pressure, after bakeout, was $\sim 1 \times 10^{-10}$ Torr. The pass energy for high-resolution XPS scans was 50 eV. Cu $2p_{3/2}$ (932.7 eV) and Au $4f_{7/2}$ (84.0 eV) core level peaks (from sputter cleaned metal foils) were used to calibrate the binding energy range of the spectrometer [12]. The precision of the binding energy (BE) measurements was ± 0.2 eV.

3. Results and Discussion

3.1. Mass spectra of $NaIO_3$

Fig. 1 shows the mass spectra produced from the same $NaIO_3$ target using 10 keV $(CsI)Cs^+$ and ~100 MeV ^{252}Cf fission fragment projectiles. Qualitatively similar mass spectra were produced by the 20 keV Cs^+ and $(CsI)_2Cs^+$ projectiles. A summary of the secondary ions sputtered from $NaIO_3$ and their measured mass to charge ratio is shown in Table 1. In general, the secondary ions can be categorized into two groups based on composition. The first contains those secondary ions composed of Na, I, and O, some of which are indicative of the composition of $NaIO_3$. The second group contains those composed of only Na and I (with the trend $(NaI)_nI^-$), and matched the composition of the secondary ions sputtered from the NaI sample. The negative ion mass spectra produced by 20 keV $(CsI)Cs^+$ projectile impacts on $NaIO_3$ and NaI are provided in Fig. 2.

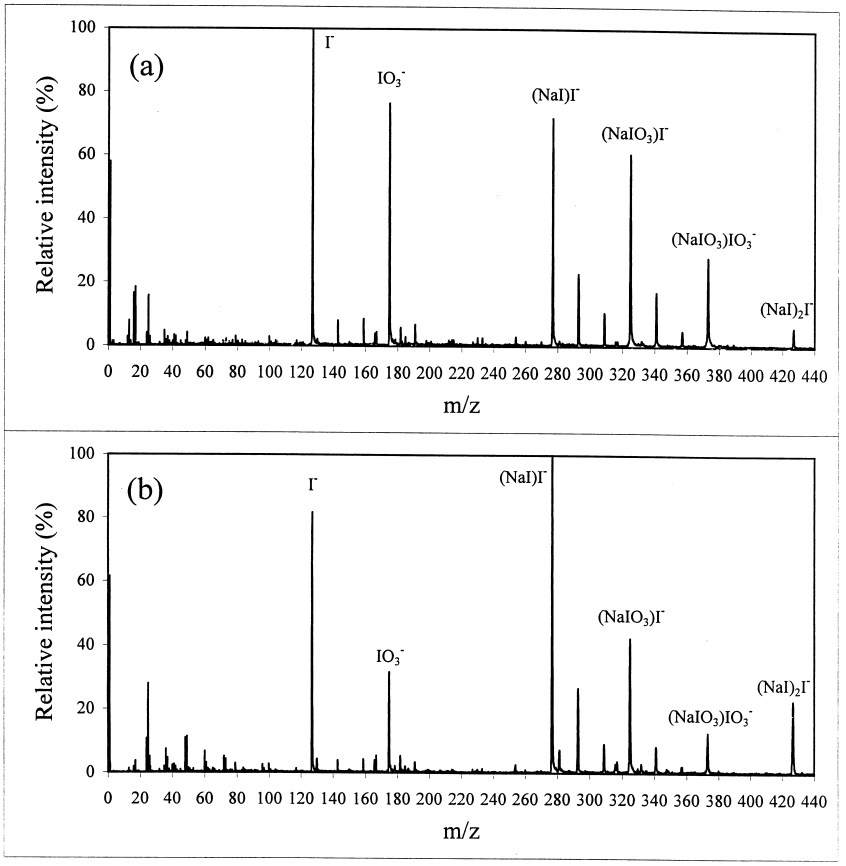

Fig. 1. Negative ion mass spectra collected from the same $NaIO_3$ target using: (a) 20 keV $(CsI)Cs^+$ projectiles (dose ~ 120 000 ions/cm^2) and (b) ~100 MeV energy ^{252}Cf fission fragments (dose ~35 000 ions/cm^2).

In the context of chemical analysis, the mass spectrum produced from $NaIO_3$ is an amalgam of secondary ion peaks characteristic of NaI and $NaIO_3$. There are two general explanations for the presence of NaI type peaks in the mass spectrum generated from $NaIO_3$. First, the iodide type peaks may arise from NaI domains that form as the aqueous $NaIO_3$ solution dries to a solid. Second, the iodide peaks may arise from recombination/rearrangement reactions that follow the impact of the primary ion. Polyatomic ion impacts have been shown to increase the production of artifact ions from tetrafluoroborate [9] and sodium nitrate [10] samples.

It is important to note that in the experiments reported here, the mass spectra were collected in the

Table 1
Secondary ions observed from Cs^+, $(CsI)Cs^+$, $(CsI)_2Cs^+$, (20 keV) and ^{252}Cf fission fragment (~100 MeV) impacts on $NaIO_3$

Mass to charge ratio[a]	Composition
127	I^-
143	IO^-
159	IO_2^-
175	IO_3^-
191	IO_4^-
277	$(NaI_2)^-$
293	$(NaI_2O)^-$
309	$(NaI_2O_2)^-$
325	$(NaI_2O_3)^-$
341	$(NaI_2O_4)^-$
357	$(NaI_2O_5)^-$
373	$(NaI_2O_6)^-$
427	$(Na_2I_3)^-$

[a] Rounded to nearest whole number.

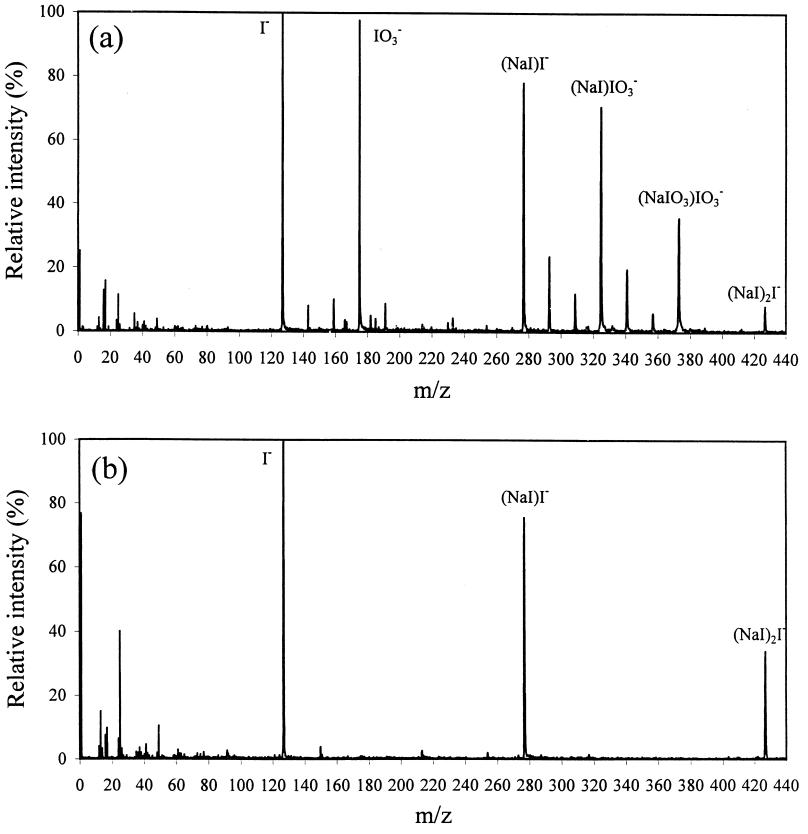

Fig. 2. Negative ion mass spectra collected from: (a) $NaIO_3$ and (b) NaI targets using 20 keV $(CsI)Cs^+$ projectiles (dose ~200 000 ions/cm^2).

event-by-event bombardment mode at the limit of single ion impacts. The dose of a given primary ion was in the range of 10^4–10^6 ions/cm^2, and the total ion dose never exceeded ~10^8 ions/cm^2. This dose is several orders of magnitude lower than the static-SIMS limit (~10^{12} ions/cm^2), the dose at which the onset of beam induced chemical damage tends to occur. The formation of and/or changes in yield of artifact ions in the mass spectra observed in these experiments are due to discrete ion impacts and not from collective effects due to high ion dose.

3.2. X-ray photoelectron spectroscopy of NaI and $NaIO_3$

To probe for the formation of NaI domains within $NaIO_3$ samples during our sample preparation procedure, we collected XPS data from individual NaI and $NaIO_3$ samples. Due to the thickness of the samples dried on the stainless steel substrates, signals from the Fe 2*p* or Cr 2*p* levels (from stainless steel) were not detected in the XPS survey scans of NaI and $NaIO_3$. Differential charging on the surfaces was observed as reported previously by Sherwood [13]. In order to correct for the charging effect, the Na 1*s* (1071.3 eV) [14] and the O 1*s* (530.0 eV) [13] core level peaks were used for sodium iodide and sodium iodate, respectively. No core level BE centers have been reported in the literature for the Na 1*s* orbital of $NaIO_3$. The BE values mentioned above were referenced to the C 1*s* level at 284.7 (± 0.2 eV) for adventitious carbon, which is the more current practice [15,16]. Fig. 3 shows the high resolution XP

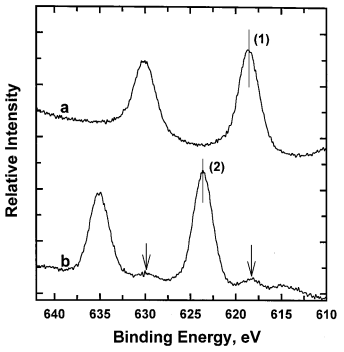

Fig. 3. High-resolution XPS scans of: (a) NaI and (b) $NaIO_3$. The numerals (1) and (2) indicate the peaks corresponding to the $3d$ $I_{5/2}$ core level for NaI and $NaIO_3$, respectively. The arrows mark the shoulders in the $NaIO_3$ XPS spectrum attributed to NaI domains.

scans of the I $3d$ core levels for NaI (a) and $NaIO_3$ (b). The BE positions of the I $3d_{5/2}$ and I $3d_{3/2}$ core levels for $NaIO_3$ were observed at 623.6 and 635.5 eV, respectively. The BE positions for the same core levels for NaI were observed at 618.5 and 629.9 eV, respectively. The I $3d$ level of $NaIO_3$ is shifted $\pm$ 5.1 eV higher relative to the I $3d$ core level of NaI as a result of greater electron density being pulled away from the I atom from the electronegative O atoms. BE positions of the $3d$ $I_{5/2}$ core levels for NaI (1) and $NaIO_3$ (2) were clearly separated, and matched those reported for them in the literature [13,14]. There is evidence in the XPS spectra of NaI present in the $NaIO_3$ sample (b) as indicated by the arrows at ~630 and 618 eV. By integrating the areas of the four peaks observed in (b), the ratio of the iodate type core levels to the iodide was 49:1. The XPS results clearly indicate that the samples prepared for ion yield measurements by allowing aqueous $NaIO_3$ to dry on stainless steel is predominantly composed of sodium iodate.

3.3. Secondary ion yield measurements at constant primary ion impact energy

Previous studies demonstrated that artifact or chemical damage ion formation by polyatomic projectiles is more sensitive to an increase in the number of atoms in the bombarding ion than the overall ion impact energy [11]. The promotion of artifact ion formation is linked to the density of the energy deposited by the primary ion in the surface region of the solid. Following impact, polyatomic primary ions fragment and deposit energy by recoil cascades. At constant impact energy, the energy deposited per unit volume is sensitive to the number of atoms in the projectile. As atoms are added to the projectile, the impact energy per constituent decreases, which in turn decreases the penetration and range of the primary ion. Energy deposited via the collision cascades initiated by each projectile constituent is distributed about a smaller volume than an equal energy atomic ion and is spatially confined to the surface region. Thus, at constant overall impact energy, the energy density scales upward as the number of atoms in the primary ion increases.

Table 2 lists the relative yields of several secondary ions produced from $NaIO_3$ by the impact of 20 keV Cs^+, $(CsI)Cs^+$, $(CsI)_2Cs^+$ projectiles. For com-

Table 2
Measured relative secondary ion yields for selected secondary ions observed from $NaIO_3$. Method for determining relative ion yields is discussed in the experimental section. The impact energy for the Cs^+, $(CsI)Cs^+$, and $(CsI)_2Cs^+$ projectile was 20 keV. The impact energy of the ^{252}Cf fission fragment was ~100 MeV

	Secondary ion					
Primary ion	I^-	IO_3^-	$(NaI)I^-$	$(NaIO_3)I^-$	$(NaIO_3)IO_3^-$	$(NaI)_2I^-$
Cs^+	1.8	.98	.22	.52	.49	.01
$(CsI)Cs^+$	9.12	9.13	8.1	8.8	4.6	0.7
$(CsI)_2Cs^+$	17.31	12.0	18.1	11.6	5.5	2.5
^{252}Cf fission fragment	12.7	5.6	19.8	8.6	2.7	5.2

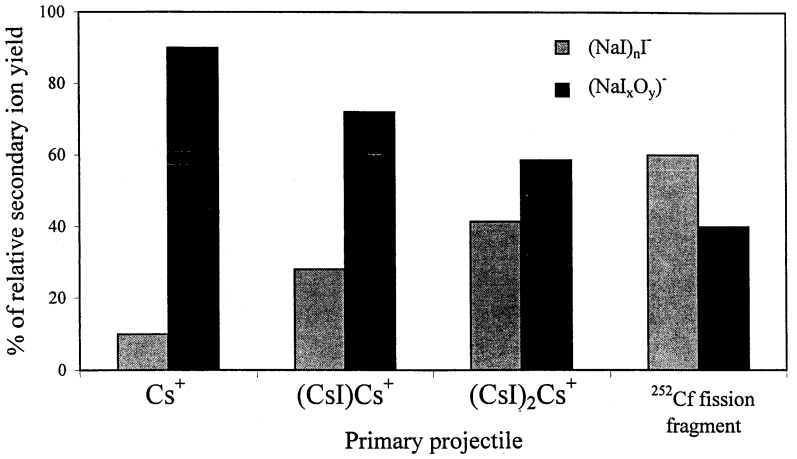

Fig. 4. Contribution to the measured ion yield (see Table 2 and accompanying text for ions used for calculation) by secondary polyatomic ions with composition $(NaI)_nI^-$ {n = 1, 2) and $(NaI_xO_y)^-$ (x = 1, 2; y = 3, 6). The $(CsI)_nCs^+$ projectiles were incident at 20 keV kinetic energy. The impact energy of the fission fragments was ~100 MeV.

parison, the yields produced by the MeV energy ^{252}Cf fission fragments are also included. Within the suite of keV energy projectiles, the secondary ion yields increase with the mass and complexity of the primary ion. The yields produced by (CsI)Cs and $(CsI)_2Cs^+$ are of the same order of magnitude of those produced by the MeV energy fission fragment, demonstrating the high sputter ion yields typical of keV polyatomic ion impacts.

Based on the XPS results, the $(NaI)_nI^-$ secondary ions observed from $NaIO_3$ are attributed to chemical damage induced by the impact of the primary ion. Of interest in this study was the quantitative change in the yield of ions corresponding to chemical damage (those with composition $(NaI)_nI^-$) relative to those representative of the $NaIO_3$ stoichiometry. To calculate the percentage of secondary ion yield characteristic of NaI and $NaIO_3$ produced by each primary projectile, the yields of: (1) $(NaI)I^-$ and $(NaI)_2I^-$ and (2) IO_3^-, $(NaIO_3)I^-$ and $(NaIO_3)IO_3^-$ were summed and divided by the sum of the secondary ion yields listed in Table 2. The yield of I^- was not included in the calculation because this secondary ion can be considered characteristic of both the iodide and iodate solids. Several additional secondary ions corresponding to the sequential addition of O to the ions listed in Table 1 were also observed in each mass spectrum. The relative yields of these peaks were low compared to those in Table 1, and their addition to the calculation described above does not significantly change the percentages reported below. Fig. 4 shows the percentage of iodide and iodate secondary ion yield produced by 20 keV energy Cs, (CsI)Cs, $(CsI)_2Cs$ ions and ~100 MeV energy fission fragments. Within the suite of keV energy ions, the yield of iodate type secondary ions decreases as projectile complexity increases. The yield of iodide type secondary ions, however, increases as the projectile complexity increases. Since the kinetic energy of each projectile was 20 keV, the relative changes in ion yield also scale with an increase in the energy density deposited. The MeV energy fission fragments, which produce fission tracks characterized by high energy density per unit volume, produce more signal characteristic of NaI than $NaIO_3$.

Increases in ion yield characteristic of ion impact induced chemical damage have been reported for sodium nitrate, sodium tetrafluoroborate, and organic molecular samples. For instance, at constant impact energy, polyatomic ions increase the yield of NO_2^- relative to NO_3^- from nitrate targets [10]. For organic targets such as polymers and polyaromatic carboxylic acids, projectiles composed of many atoms, such as

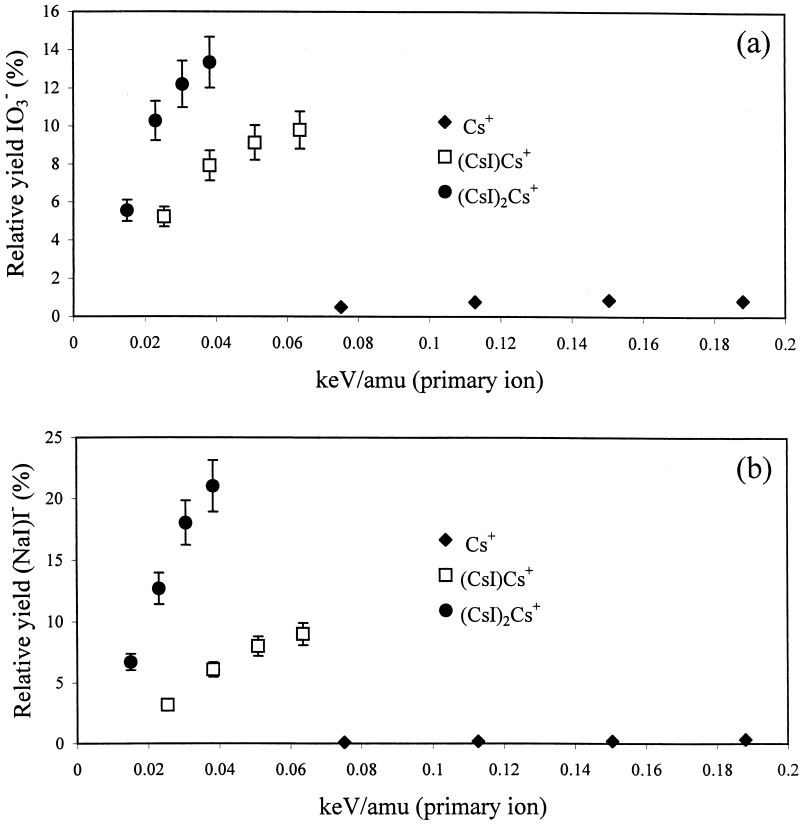

Fig. 5. Relative yields of: (a) IO_3^- and (b) $(NaI)I^-$ sputtered from $NaIO_3$ by Cs, (CsI)Cs, and $(CsI)_2Cs$ primary ions. Yields are plotted as a function of energy per projectile mass unit, which is proportional to the square of the projectile velocity.

C_{60}^+ produce as much chemical damage (measured using hydride attached carbon cluster anions), per projectile impact, as ^{252}Cf fission fragments [17,18].

3.4. Secondary ion yield measurements from $(CsI)_nCs^+$ impacts at 10–25 keV

To determine the influence of projectile velocity on secondary ion yields from $NaIO_3$, the Cs, (CsI)Cs, and $(CsI)_2Cs$ projectiles were accelerated to impact energies ranging from 10 to 25 keV. Fig. 5 shows the relative yield of IO_3^- (a) and $(NaI)I^-$ (b) plotted as a function of the kinetic energy per mass unit of the primary ion, which is proportional to the square of the projectile velocity. Fig. 6 shows the relative yield of $(NaIO_3)IO_3^-$ (a) and $(NaI)_2I^-$ (b) versus the energy per mass unit of the primary ion. For each primary ion, the secondary ion yields increase with the square of the projectile velocity.

Nonlinear yield enhancements in secondary ion yields from a variety of organic, inorganic, and metallic targets have been reported in sputtering experiments using Au_n^+ [5], $(CsI)_nCs^+$ [19], $(La_2O_3)_nLaO^+$ [3], and Ta_n^+ [20] projectiles. A nonlinear enhancement exists when the yield per projectile atom produced by a cluster projectile composed of *n* constituents is greater than the sum of the yields produced by the impact of *n* atomic projectiles when compared at the same incident velocity. The enhanced ion yields are attributed to the high energy density deposited into nanoscale volumes of the solid surface by polyatomic projectiles. Molecular dynamics simulations suggest

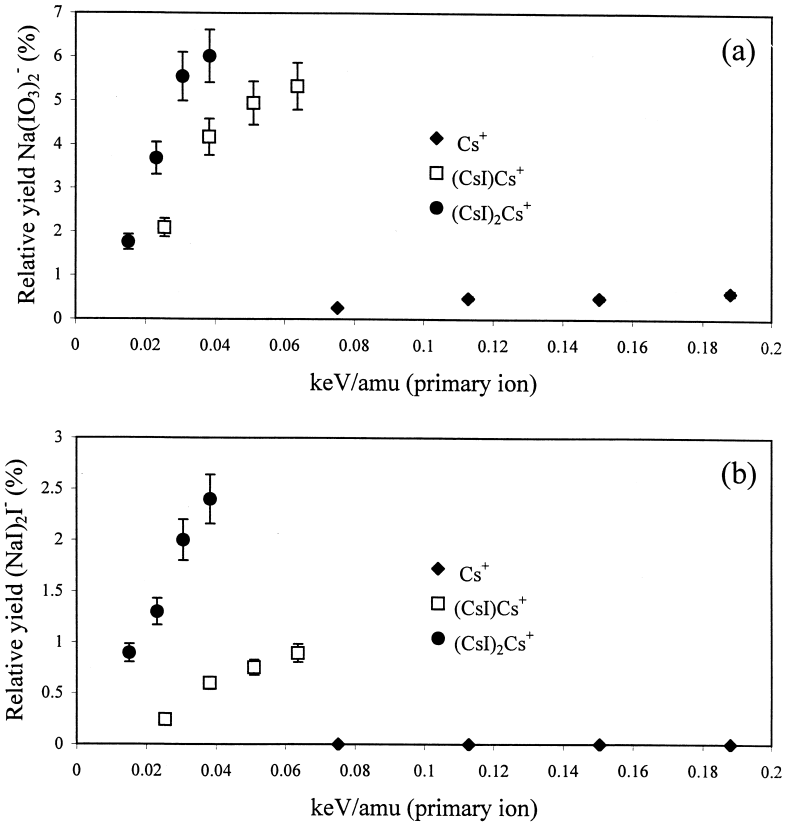

Fig. 6. Relative yields of: (a) $(NaIO_3)IO_3^-$ and (b) $(NaI)_2I^-$ sputtered from $NaIO_3$ by Cs, (CsI)Cs, and $(CsI)_2Cs$ primary ions. Yields are plotted as a function of energy per projectile mass unit, which is proportional to the square of the projectile velocity.

that multiple overlapping collision cascades, each created by individual projectile atoms, act in concert to eject polyatomic species from the surface [21,22].

To probe ion yield enhancements from $NaIO_3$, the secondary ion yields produced by the $(CsI)_nCs$ primary ions were divided by the number of atoms in the bombarding projectile (the difference in mass of Cs and I is small and the cluster is thus considered homogeneous). Figs. 7 and 8 show the yield of IO_3^- (7a) $(NaI)I^-$ (7b), $(NaIO_3)IO_3^-$ (8a), and $(NaI)_2I^-$ (8b), per projectile constituent, versus the energy per mass unit of the bombarding ion. Because of limitations to the primary ion kinetic energies accessible in the current instrument configuration, Cs^+ could not be directly compared to the polyatomic primary ions at the same incident velocity. Considerable deflection of the primary ion trajectory occurs at impact energies below 10 keV, causing a change in the angle of incidence. Secondary ion yields scale with $1/\cos^2\theta$, where θ is the angle of incidence. Assuming that the yield trend produced by Cs^+ remains linear at lower velocities, it is clear from Figs. 7 and 8 that the ion yields *per projectile constituent* increase nonlinearly from Cs^+ to $(CsI)Cs^+$. As shown in Figs. (7a) and (8a), no further increase in the yield of IO_3^- or $(NaIO_3)IO_3^-$ per projectile atom is observed progressing from $(CsI)Cs^+$ to $(CsI)_2Cs^+$. The yield per constituent for $(NaI)I^-$ and $(NaI)_2I^-$ (7b) and (8b), however, continues to increase using $(CsI)_2Cs^+$ over $(CsI)Cs^+$.

The secondary ions characteristic of the iodate composition and those due to chemical damage both

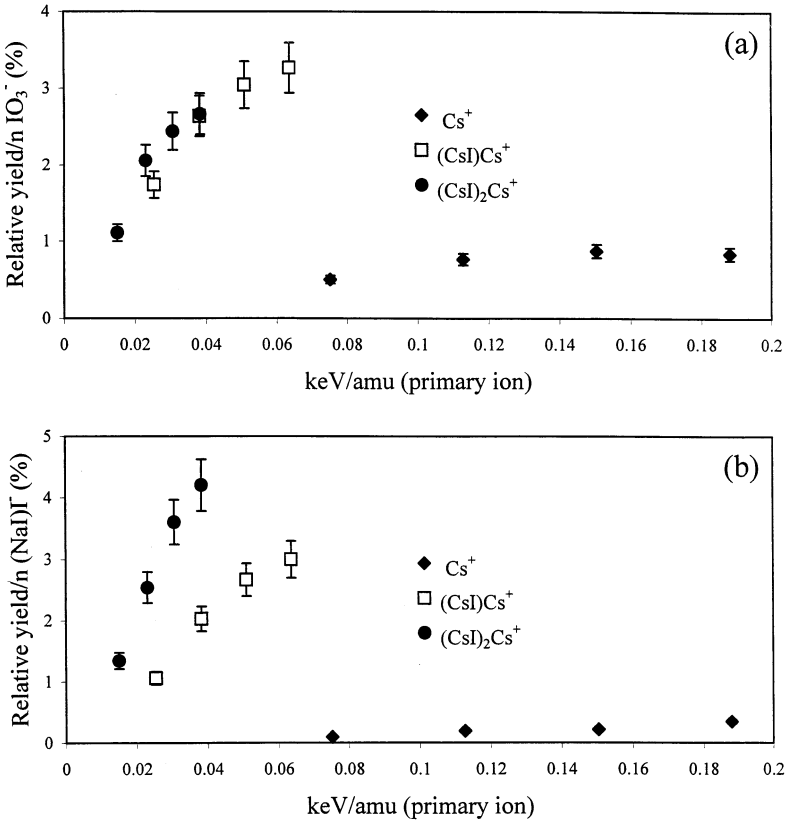

Fig. 7. Relative yields of: (a) IO_3^- and (b) $(NaI)I^-$ sputtered from $NaIO_3$ by Cs, (CsI)Cs, and $(CsI)_2Cs$ primary ions. The yields are divided by the number of Cs and I atoms in the bombarding ion to demonstrate yield per projectile constituent.

increase nonlinearly when (CsI)Cs is used as a primary ion instead of Cs, i.e. the yield produced by $(CsI)Cs^+$ is greater than three times they yield produced by Cs^+. The yield enhancement for IO_3^- and $(NaIO_3)IO_3^-$ saturates at the three atom projectile, and the yield per constituent produced by $(CsI)_2Cs^+$ scales linearly with the increase in projectile complexity. Le Beyec and co-workers measured the saturation of nonlinear enhancements in ion yields from organic targets [23]. In their study, which involved carbon based primary projectiles, the nonlinear increase in yield of deprotonated molecule ions from a phenylalanine target ceased at $n = 7$. Beyond seven atoms, secondary ion yields increased linearly with the addition of projectile constituents. Similar results have been obtained in our laboratory using $(La_2O_3)_nLaO^+$ projectiles [3].

To our knowledge, this is the first case in which secondary ions with two different compositions that originate from the same inorganic compound show distinct behavior in yield enhancement saturation. The possibility that the observed saturation is an artifact introduced by secondary ion multiplicity was checked. It may be recalled that qualitative measurements based on the pulse counting technique are only valid if the probability of ion multiplicity based on Poisson statistics is small. Ion multiplicity is defined here as the number of ions of the same *m/z* value sputtered by the same primary ion impact. With this in mind, the transmission of the secondary ion ToF region was decreased by an additional 50% using low transmission grids. The yields of IO_3^-, $(NaIO_3)IO_3^-$, $(NaI)I^-$, and $(NaI)_2I^-$ at primary ion impact energies of 10–25 keV were then remeasured. The yield trends displayed

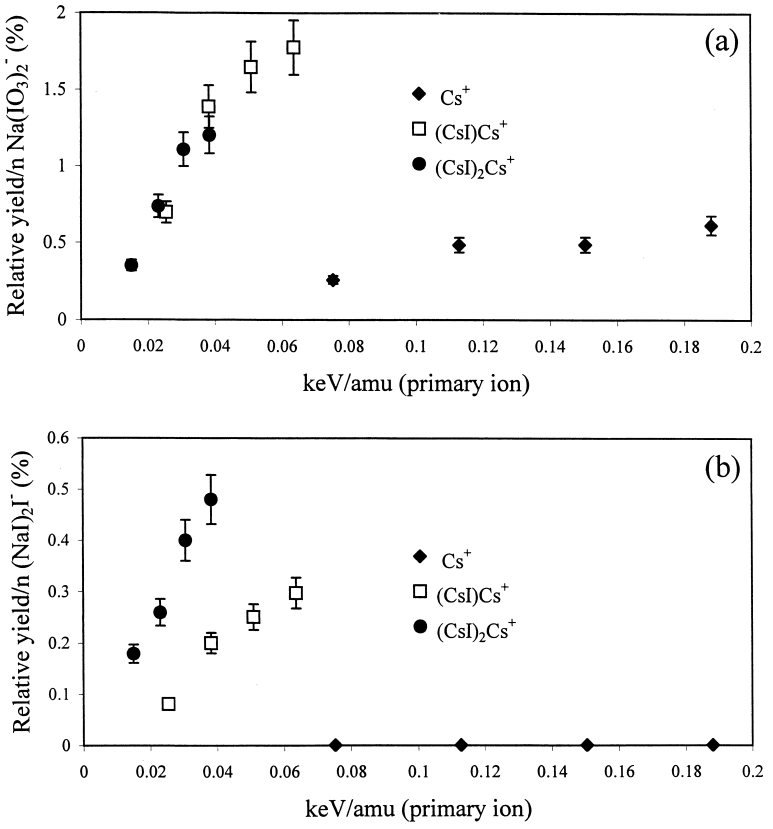

Fig. 8. Relative yields of: (a) $(NaIO_3)IO_3^-$ and (b) $(NaI)_2I^-$ sputtered from $NaIO_3$ by Cs, (CsI)Cs, and $(CsI)_2Cs$ primary ions. The yields are divided by the number of Cs and I atoms in the bombarding ion to demonstrate yield per projectile constituent.

in Figs. 7 and 8 were reproduced, with the concomitant reduction of the relative yields of all secondary ions due to the decrease in transmission efficiency of the instrument. The saturation of the yield enhancement of IO_3 and $(NaIO_3)IO_3^-$ is therefore considered to be real and due to chemical effects occurring during ion formation following the impact of the polyatomic primary ions.

4. Conclusions

By using XPS and SIMS with atomic and polyatomic projectiles, we have shown that the formation of $(NaI)_nI$ negative ions from sodium iodate is due to chemical damage created by individual primary ion impacts. It is clear from the comparison of atomic and polyatomic primary projectile impacts at equal kinetic energy that the increase in chemical damage scales with an increase in energy density, as has been shown in earlier experiments employing $(CsI)_nCs^+$ projectiles incident on sodium tetrafluoroborate [9] and nitrate targets [10]. It is interesting to note that the polyatomic projectiles increase the relative abundance of secondary ions that reflect reduction reactions during ion formation. One possible explanation for the increase in iodide-type ion yield might be an increase in secondary electron production within the zone of high collisional excitation induced within the solid by a polyatomic projectile impact. For instance, the chemical reduction of iodate (I oxidation state of +5) to iodide is a process that requires six electrons. The yields of electrons ejected from surfaces by

cluster impacts in the keV and MeV energy range have been measured [24–26]. While the secondary electron emission yields produced by cluster ion impacts are higher than atomic projectile impacts at similar incident velocities, the yield increase is sub-linear (electron yield per constituent decreases) with respect to the number of projectile atoms. Less is known, however, about the production and propagation of secondary electrons *within* the solid, and the subsequent bond breakage and reduction induced by polyatomic ion impacts. While the present study provides only circumstantial evidence for the role of secondary electrons, studies of the interaction of ionizing radiation with alkali nitrate solids have implicated secondary electron production within the solid as the cause of nitrate anion dissociation [27].

In any case, the results presented here have broad implications on the use of polyatomic primary ions to characterize the surfaces of complex inorganic systems such as superconductors, mineral, or clay materials. Polyatomic projectiles, while increasing the yield of secondary ions by factor of 10–100, cause a significant increase in ion signal characteristic of chemical damage at the level of discrete ion impacts. Based on the XPS data and the low ion doses used in these experiments, we can conclude that the increases in artifact ion production are due to the simultaneous impact of several projectile constituents on a localized area of the solid surface. Surface characterization of inorganic materials using cluster projectile bombardment will require a firm understanding of the reactions that take place during ion formation, and the proper choice of primary ion. In the case of $(CsI)_nCs^+$ impacts on sodium iodate, the best combination of high analytically useful ion yield and least chemical damage is produced by the three atom cluster projectile.

Acknowledgements

This work was supported by the National Science Foundation (M.J.V., V.S., E.A.S.), the U. S. Department of Energy, Office of Basic Energy Sciences, Division of Chemical Sciences and the Robert A. Welch Foundation (D.W.G.). C.C.C. gratefully acknowledges support from the Associated Western Universities, Inc. and Pacific Northwest National Laboratories operated by Battelle Memorial.

References

[1] A. Benninghoven, B. Hagenhoff, E. Niehuis, Anal. Chem. 65 (1993) 630A, and references cited therein.
[2] M.J. Van Stipdonk, R.D. Harris, E.A. Schweikert, Rapid Commun. Mass Spectrom. 10 (1996) 1987.
[3] R.D. Harris, M.J. Van Stipdonk, E.A. Schweikert, Int. J. Mass Spectrom. Ion Processes 174 (1998) 167.
[4] A.D. Appelhans, J.E. Delmore, Anal. Chem. 61 (1989) 1087.
[5] M. Benguerba, A. Brunelle, S. Della-Negra, J. Depauw, H. Joret, Y. Le Beyec, M.G. Blain, E.A. Schweikert, G. Ben Assayag, P. Sudraud, Nucl. Instrum. Methods Phys. Res. B 62 (1991) 8.
[6] F. Kötter, E. Niehuis, A. Benninghoven, SIMS XI, Wiley, Chichester, 1998, p. 459.
[7] F. Kötter, A. Benninghoven, Appl. Surf. Sci. 133 (1998) 47.
[8] S. Roberson, G. Gillen, Rapid Commun. Mass Spectrom. 12 (1998) 1303.
[9] M.J. Van Stipdonk, R.D. Harris, E.A. Schweikert, Rapid Commun. Mass Spectrom. 11 (1997) 1794.
[10] M.J. Van Stipdonk, D.R. Justes, V. Santiago, E.A. Schweikert, Rapid Commun. Mass Spectrom. 12 (1998) 1639.
[11] M.G. Blain, S. Della-Negra, H. Joret, Y. Le Beyec, E.A. Schweikert, J. Vac. Sci. Technol. A8 (1990) 2265.
[12] M.P. Seah, Surf. Interface Anal. 14 (1989) 488.
[13] P.M.A. Sherwood, J. Chem. Soc. Faraday Trans. II 72 (1976) 1805.
[14] W.E. Morgan, J.R. Van Wazer, W.J. Stec, J. Am. Chem. Soc. 95 (1973) 751.
[15] T.L. Barr, S. Seal, J. Vac. Sci. Technol. A13 (1995) 1239.
[16] T.L. Barr, Modern ESCA, CRC, Boca Raton, FL, 1994, Chap. 6 and references cited therein.
[17] C.W. Diehnelt, M.J. Van Stipdonk, R.D. Harris, E.A. Schwiekert, in Secondary Ion Mass Spectrometry, SIMS XI, G. Gillen, R. Lareau, J. Bennett, F. Stevie (Eds.), Wiley, Chichester, 1998, p. 593.
[18] C.W. Diehnelt, M.J. Van Stipdonk, E.A. Schweikert, Phys. Rev. A 59 (1998) 4470.
[19] M.G. Blain, S. Della-Negra, H. Joret, Y. Le Beyec, E.A. Schweikert, Phys. Rev. Lett. 63 (1989) 1625.
[20] S.F. Belykh, V.I. Matveev, U. Kh. Rasulev, A.V. Samartsev, I.V. Veryovkin, in Secondary Ion Mass Spectrometry, SIMS XI, G. Gillen, R. Lareau, J. Bennett, F. Stevie (Eds.), Wiley, Chichester, 1998, p. 957.
[21] R. Žarić, B. Pearson, K.D. Krantzman, B.J. Garrison, Int. J. Mass Spectrom. Ion Processes 174 (1998) 155.
[22] R. Žarić, B. Pearson, K.D. Krantzmann, B.J. Garrison, in Secondary Ion Mass Spectrometry, SIMS XI, G. Gillen, R. Lareau, J. Bennett, F. Stevie (Eds.), Wiley, Chichester, 1998, pp. 601–4.
[23] K. Boussofiane-Baudin, G. Bolbach, A. Brunelle, S. Della-

Negra, P. Håkansson, Y. Le Beyec, Nucl. Instrum. Methods Phys. Res. B 88 (1994) 160.
[24] K. Baudin, A. Brunelle, J. Depauw, S. Della-Negra, Y. Le Beyec, E. Parilis, Nucl. Instrum. Methods Phys. Res. B 117 (1996) 47.
[25] R. Moshammer, R. Matthäus, J. Phys. Coll. C2, 50 (1989) 111.
[26] A. Brunelle, P. Chaurand, S. Della-Negra, Y. Le Beyec, E. Parilis, Rapid Commun. Mass Spectrom. 11 (1997) 353.
[27] J-J. Shin, S.C. Langford, J.T. Dickinson, Y. Wu, Nucl. Instrum. Methods Phys. Res. B 193 (1995) 284.